EARTH SURFACE PROCESSES AND LANDFORMS
Earth Surf. Process. Landforms (2010)
Copyright © 2010 John Wiley & Sons, Ltd.
Published online in Wiley InterScience
(www.interscience.wiley.com) DOI: 10.1002/esp.1914

Characterization of complex fluvial systems using remote sensing of spatial and temporal water level variations in the Amazon, Congo, and Brahmaputra Rivers

Hahn Chul Jung[1], James Hamski[2], Michael Durand[3]*, Doug Alsdorf[1,3,4], Faisal Hossain[5], Hyongki Lee[1], A. K. M. Azad Hossain[6], Khaled Hasan[7], Abu Saleh Khan[8] and A.K.M. Zeaul Hoque[8]

[1] School of Earth Sciences, Ohio State University, Columbus OH
[2] The Louis Berger Group, Inc., Needham MA
[3] Byrd Polar Research Center, Ohio State University, Columbus OH
[4] The Climate, Water, and Carbon Program of OSU
[5] Department of Civil and Environmental Engineering, Tennessee Technological University, Cookeville, TN
[6] National Center for Computational Hydrosciences and Engineering, University of Mississippi, Oxford, MS
[7] Department of Geology, Dhaka University, Bangladesh
[8] Institute of Water Modeling, Dhaka, Bangladesh

Received 12 January 2009; Revised 10 July 2009; Accepted 18 August 2009

*Correspondence to: Michael Durand, Byrd Polar Research Center, Ohio State University, 108 Scott Hall, 1090 Carmack Road, Columbus, OH 43210-1808, USA.
Email: durand.8@osu.edu

ESPL
Earth Surface Processes and Landforms

ABSTRACT: The Surface Water and Ocean Topography (SWOT) satellite mission will provide global, space-based estimates of water elevation, its temporal change, and its spatial slope in fluvial environments, as well as across lakes, reservoirs, wetlands, and floodplains. This paper illustrates the utility of existing remote sensing measurements of water temporal changes and spatial slope to characterize two complex fluvial environments. First, repeat-pass interferometric SAR measurements from the Japanese Earth Resources Satellite are used to compare and contrast floodplain processes in the Amazon and Congo River basins. Measurements of temporal water level changes over the two areas reveal clearly different hydraulic processes at work. The Amazon is highly interconnected by floodplain channels, resulting in complex flow patterns. In contrast, the Congo does not show similar floodplain channels and the flow patterns are not well defined and have diffuse boundaries. During inundation, the Amazon floodplain often shows sharp hydraulic changes across floodplain channels. The Congo, however, does not show similar sharp changes during either infilling or evacuation. Second, Shuttle Radar Topography Mission measurements of water elevation are used to derive water slope over the braided Brahmaputra river system. In combination with *in situ* bathymetry measurements, water elevation and slope allow one to calculate discharge estimates within 2·3% accuracy. These two studies illustrate the utility of satellite-based measurements of water elevation for characterizing complex fluvial environments, and highlight the potential of SWOT measurements for fluvial hydrology. Copyright © 2010 John Wiley & Sons, Ltd.

KEYWORDS: hydrology; remote sensing; river; synthetic aperture radar

Introduction

Remote sensing estimates of river stage have been achieved via radar altimetry (Koblinsky *et al.*, 1993; Birkett *et al.*, 2002; Kouraev *et al.*, 2004; Frappart *et al.*, 2005, 2008; Calmant and Seyler, 2006; Leon *et al.*, 2006;), but estimates are subject to significant limitations: spatial footprints are on the order of several kilometers, and spatial gaps in coverage are substantial (Alsdorf *et al.*, 2007). To overcome the limitations of existing remote sensing instruments, Alsdorf *et al.* (2007) describe the need for an imaging (or wide swath) interferometric synthetic aperture radar (SAR) altimeter to measure water surface elevations. The proposed satellite mission has been named the Surface Water and Ocean Topography mission (SWOT), and has been recommended by the National Research Council Decadal Survey (NRC, 2007) to measure ocean topography as well as water elevation over land; the launch date timeframe proposed by the NRC is 2013–2016. The SWOT instrument would provide global sampling of fluvial environments with average channel widths greater than 50 m, and would achieve precision of a few centimeters when averaged over ~1 km^2 of river area. The technology for SWOT is a Ka-band radar interferometer, as described by Alsdorf *et al.* (2007). SWOT water surface elevation measurements (h) will yield highly accurate

estimates of the temporal variations ($\partial h/\partial t$) and spatial variations ($\partial h/\partial x$) of water levels. It is expected that these new measurements will lead to fundamentally new insights into the two-dimensional hydraulic processes that govern complex fluvial environments.

In this paper, we present two illustrations of the use of $\partial h/\partial t$ and $\partial h/\partial x$ measurements available via existing sensors to characterize complex fluvial environments. First, we present a case in which the coupled river-floodplain environment is characterized using measurements of $\partial h/\partial t$ derived from repeat-pass interferometric SAR from the Japanese Earth Resources Satellite-1 (JERS-1). The method is applied over portions of the Amazon River and the Congo River, revealing substantive differences in the fluvial hydraulic processes at work in the two regions. Second, we present a case in which the discharge in the braided Brahmaputra River is characterized using the Shuttle Radar Topography Mission (SRTM) measurements of $\partial h/\partial x$. Together, these case studies illustrate the utility of existing remote sensing for characterizing complex and large fluvial environments.

Floodplain Characterization Using JERS-1 SAR Interferometry for the Amazon and Congo

Water flow through wetlands controls a number of processes including changes in stored water, biogeochemical cycling, sediment delivery, and nutrient exchange. The floodplains and wetlands of the Amazon and Congo rivers are massive in size and in volumetric fluxes. The Amazon Basin, with an area of ~6·0 M km^2 and containing the largest tropical rainforest in the world, contributes 15% to 20% of the global river discharge to the oceans (annually averaged discharge of ~200 000 m^3 s^{-1}). The Congo River is the second-largest river globally, both in terms of discharge (~40 600 m^3 s^{-1} annual average) and basin area (~3·5 M km^2).

Despite its global importance as the second-largest river, the Congo has been the subject of far fewer research studies than the Amazon (Laraque *et al.*, 2001 represents one of the few Congo studies). Most of the primary research on the Congo swamps and wetlands dates from the colonial era (Campbell, 2005) with a limited number of surface water hydrology publications since then. In contrast, *in situ* measurements coupled with improvements in remote sensing (Birkett *et al.*, 2002; and see references in Alsdorf *et al.*, 2006) and modeling techniques have added significantly to our measurement and hydrologic mass-balance knowledge in the Amazon Basin (Alsdorf, 2003).

In this section, repeat-pass interferometric SAR measurements are utilized to characterize and map $\partial h/\partial t$ over a section of the floodplains of both the Congo and Amazon rivers. These maps allow the Congo and Amazon floodplains to be compared and contrasted, which lead to new insights about their respective structures.

Study areas

The study areas within the Congo and Amazon basins are shown in Figure 1. The mainstem Amazon River floodplain in Brazil is located between terraces near the Japura and Solimoes Rivers, and covers approximately 92 000 km^2 (Sippel *et al.*, 1992). The floodplains of the Amazon and its tributaries are built from overbank deposits with an overall annually inundated area of about 750 000 km^2 (Melack and Forsberg, 2001). The mainstem floodplain is built from the fluvial delivery of sediments and reworking over a few thousand years by the migration of both the Amazon River and floodplain channels (Mertes *et al.*, 1996). Discrete, episodic events delivering pulses of sediment are evident in portions of the floodplain several kilometers distal from the mainstem (Aalto *et al.*, 2003).

Congo wetlands are known as swamp forests located mostly in broad topographic depressions of the central basin interfluvial regions. The Congo Basin is uniquely located with respect to the Inter-Tropical Convergence Zone (ITCZ) such that precipitation peaks occur twice annually (Kazadi and Kaoru, 1996). Study locations on the Ubangui and Mossaka rivers receive their major precipitation peaks in October/November (see flood wave peak for C1, Figure 2) whereas rivers draining the southern half of the basin tend to receive their peaks in March/April. Essentially, because the Congo Basin drains from both the Northern and Southern Hemispheres, it does not have great seasonal fluctuations in water level as does the Amazon River (compare C2 with A1, Figure 2). The Amazon study area is at the confluence of Solimoes and Japura rivers whereas the

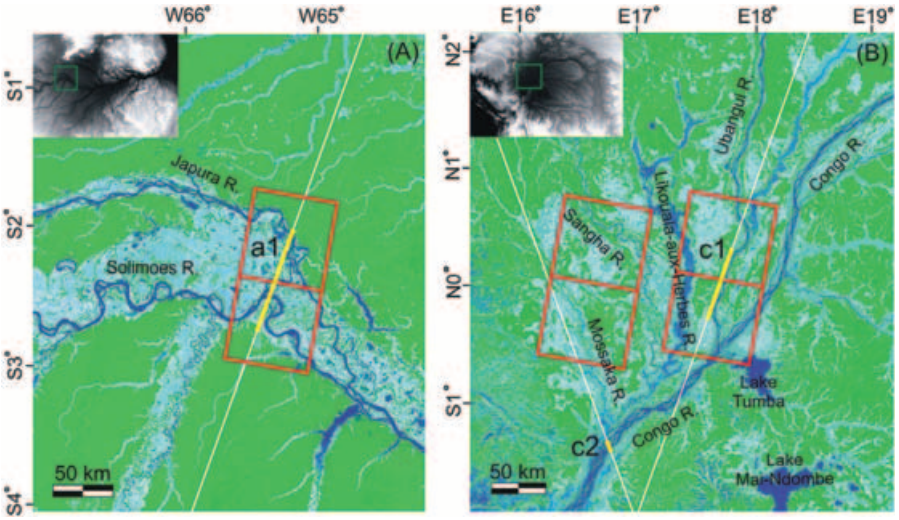

Figure 1. The (A) Amazon and (B) Congo study areas shown using overlays of the low and high water GRFM mosaics. Light blue marks seasonally flooded areas; green is non-flooded areas; dark blue is indicative of areas that always contain water, e.g. river channels. Topex/Poseidon altimetric measurements are marked with yellow and white lines. Red diagonal boxes locate JERS-1 SAR swaths. This figure is available in colour online at www.interscience.wiley.com/journal/espl

Copyright © 2010 John Wiley & Sons, Ltd.

DOI: 10.1002/esp

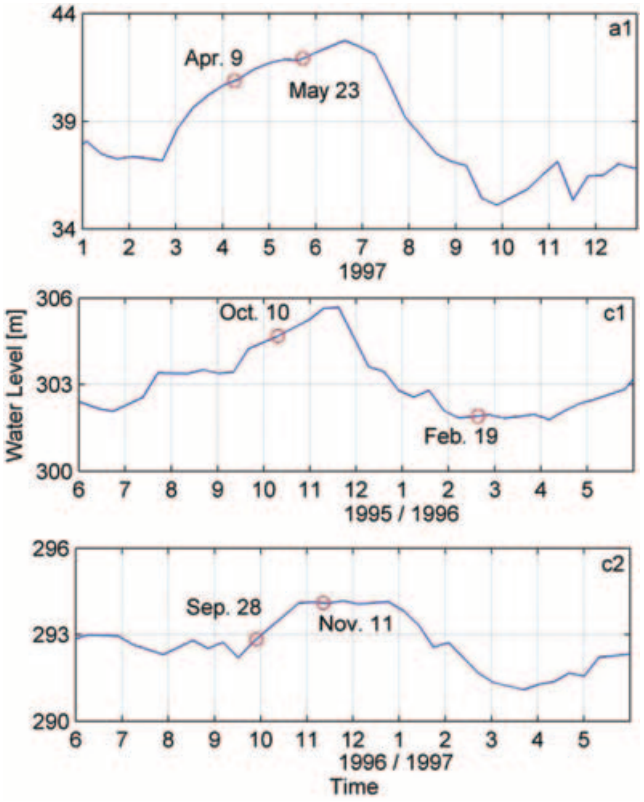

Figure 2. Water surface heights derived from Topex/Poseidon altimetry. See Figure 1 for locations. X axis numbers refer to months where 1 is January, 2 is February, etc. and y axis numbers refer to orthometric heights with respect to EGM96 geoid model. Dates of interferometric pairs are noted. Lines a1, c1, and 2 correspond to 143, 114, and 18 altimetric points (yellow in Figure 1), respectively. This figure is available in colour online at www.interscience.wiley.com/journal/espl

study area in Congo includes the central part of the Congo basin, which is often called the Cuvette Congolaise (literally, 'saucer,' or 'shallow bowl', Figure 1) and is an immense depression containing Quaternary alluvial deposits that rest on thick sediments of continental origin, consisting principally of sands and sandstones (Sautter, 1966).

Data and methods

The Global Rain Forest Mapping project (GRFM, De Grandi *et al.*, 2000) provided regional JERS-1 SAR amplitude mosaics at both high and low water seasons in the Amazon and Congo Basins. The GRFM mosaics over the central Amazon Basin were acquired during the low-water period of September/November 1995 and during the high-water period of May/June 1996 whereas the GRFM mosaics over central Africa were acquired during the low-water period of January–March 1996 and during the high-water period October/November 1996.

Interferometric SAR processing

Interferometric JERS-1 SAR processing followed the 'two pass' method (Massonnet *et al.*, 1993). Raw scenes with the same path were concatenated, and after flat-earth phase removal, the interferometric phase includes the topographic relief as well as any changes in the radar range (i.e. water level change (Alsdorf *et al.*, 2000)). The topographic-related phase was subtracted using the C-band SRTM elevation data to make differential interferograms having phase values indicative of wetland water level changes. The short perpendicular baselines (Table 1) and the C-band SRTM relative height errors of 5·5 m (Farr *et al.*, 2007) cause less than 0·44 radians of phase change based on the topography and baseline relationship. The resultant error is equivalent to 0·8 cm in the line-of-sight direction or 1·0 cm of water level change (i.e. vertical component).

The SAR backscatter coefficient was used to differentiate between flooded vegetation, non-flooded areas, and open-water in river channels. Flooded vegetation in JERS-1 amplitude images yields brighter returns than non-flooded areas because the radar pulse is returned to the antenna when it reflects from water surfaces and scatters from inundated vegetation (i.e. the 'double bounce effect'). In contrast, open-water river channels show little backscattering return, i.e. a specular reflection at L-band. The radiometric accuracy is considered sufficient for regional scale applications (Rosenqvist and Birkett, 2002). To reduce range dependencies in the backscatter strength, we calculated the average σ^0 in each range bin, subtracted the linear trend of the averaged σ^0 and added the mean of the linear trend. After performing the radiometric correction, the JERS study scenes display a backscatter response that is consistent over the entire range of incidence angles. Siqueira *et al.* (2003) give a simple classification and interpretation guide of multi-season JERS-1 SAR data for scattering mechanisms in which the 'double bounce' of flooded vegetation is greater than –5·5 dB and the noise floor of open water and bare ground is less than –15 dB. Jung and Alsdorf (in press) showed that, in the Amazon basin, flooded and non-flooded areas have a mean interferometric coherence greater than 0·1, including ~4 year temporal baselines, whereas open-water river channels have a mean coherence which is consistently less than 0·1. Thus, in our study we classified the pixels having backscatter brighter than –5·5 dB and interferometric coherence greater than 0·1 as flooded areas.

Measurements of changes in water levels ($\partial h/\partial t$) were obtained by unwrapping the differential phases of flooded areas with minimum cost flow techniques and a triangular irregular network. In the phase unwrapping stage, adaptive radar interferogram filtering was applied to reduce noise and enhance fringe visibility. After removal of the topographic phase ('two pass' method), the remaining differential phase depends on water level changes in the flooded areas and on any remaining, uncorrected topographic phase. Because non-flooded areas do not show water level changes, their

Table 1. Description of satellite data used for Congo and Amazon

		Amazon		Congo
JERS-1 SAR	Perp. baseline	195 m	97 m	621 m
	Ambiguity height	229 m/2 pi	463 m/2 pi	72 m/2 pi
	Date	April 9, 1997	Oct. 10, 1995	Sept. 28, 1996
		May 23, 1997	Feb. 19, 1996	Nov. 11, 1996
	Time interval	44 days	132 days	44 days
Topex/Poseidon	Water level change	+103 cm	–278 cm	+126 cm
Landsat	Date	Oct. 18, 1986	Feb. 18, 2001	Feb. 12, 2002

Copyright © 2010 John Wiley & Sons, Ltd.

DOI: 10.1002/esp

differential phase is essentially zero. We take this as an indication that any uncorrected topographic phase over the flooded areas is also negligible. Taking into account the wavelength and incidence angle of the JERS-1 SAR images (Alsdorf *et al.*, 2000), interferometrically measured water level changes in the direction of the radar line-of-sight are converted to a vertical displacement where 1·0 radian of interferometric phase is equivalent to 2·4 cm of purely vertical height change.

Altimetry measurements

The interferometric SAR measurements provide relative changes in water levels and thus require a reference datum to convert to absolute values (Alsdorf *et al.*, 2007). In this study, Topex/Poseidon altimetry measurements are used for the reference datum. Topex ellipsoidal heights are converted to orthometric heights with respect to the WGS84 reference system using the EGM96 geoid model. We spatially average Topex 10 Hz retracked data using the modified 50% threshold retracker (Lee *et al.*, 2008) over a distance corresponding to the intersection between the satellite ground track and water body (i.e. A1, C1, and C2 yellow lines in Figure 1) to construct a time series (Figure 2). While a water mask (Hess *et al.*, 2003) is used to identify the altimeter returns from Amazon water surfaces, we defined Congo River or wetland waveforms as those that have automatic gain control values larger than 45 dB. The mean RMSEs of A1, C1, and C2 altimetric measurements are 16, 14, and 12 cm, respectively. Table 1 presents altimeter measured water level changes, i.e. datums. In the Amazon and along the Ubangui River in the Congo, these are reliable indicators of the datum, given the altimetric location in the center of the JERS-1 scenes and with a timing coincident with the acquisitions of the interferometric pair. Along the Mossaka and Sangha Rivers, the datum is less reliable because the altimetric location is 70 km south of the JERS-1 scenes.

Results and discussion

Following the methods described in the previous section, maps of $\partial h/\partial t$ were extracted over the study areas in the Amazon and Congo River basins; these maps are shown in Figure 3.

Amazon floodplain characterization

From Figure 3, there is an overall pattern of increasing $\partial h/\partial t$ from upstream to downstream. However, within this broad trend, there is substantial spatial variability; a subset of the interfluvial area marked 'R1' in Figure 3 is shown in Figure 4. As pointed out by Alsdorf *et al.* (2007), mass continuity suggests that a greater amount of water is flowing to floodplain pockets with a greater $\partial h/\partial t$, compared with locations of smaller $\partial h/\partial t$. Directions of water flow inferred from spatial variations in $\partial h/\partial t$ are shown as black arrows. From the disparate flow directions shown in R1 in Figure 4, it is clear that patterns of $\partial h/\partial t$ on the Amazon floodplain are spatially complex. Moreover, distinct boundaries between pockets of small and large $\partial h/\partial t$ values can be identified.

Following Alsdorf *et al.* (2007), we hypothesize that these boundaries are associated with floodplain channels. These sinuous, convoluted, and interconnected floodplain channels are clearly evident in the Landsat and JERS-1 SAR imagery shown in Figure 4. Identifying these channels using SRTM elevations is more complex. For instance, there does not appear to be a straightforward relationship between topography and the $\partial h/\partial t$ pattern; i.e. lower (higher) elevations do not appear to be associated with greater (lesser) $\partial h/\partial t$. Moreover, in the SRTM DEM, floodplain channels are often flanked by anomalously high elevations most likely indicative of C-band radar returns from the forest canopy rather than the underlying floodplain topography. Nonetheless, sharp changes in the interferometric SAR $\partial h/\partial t$ measurements coincide with floodplain channels; this can be seen by examining the transect profile P1 in Figure 4.

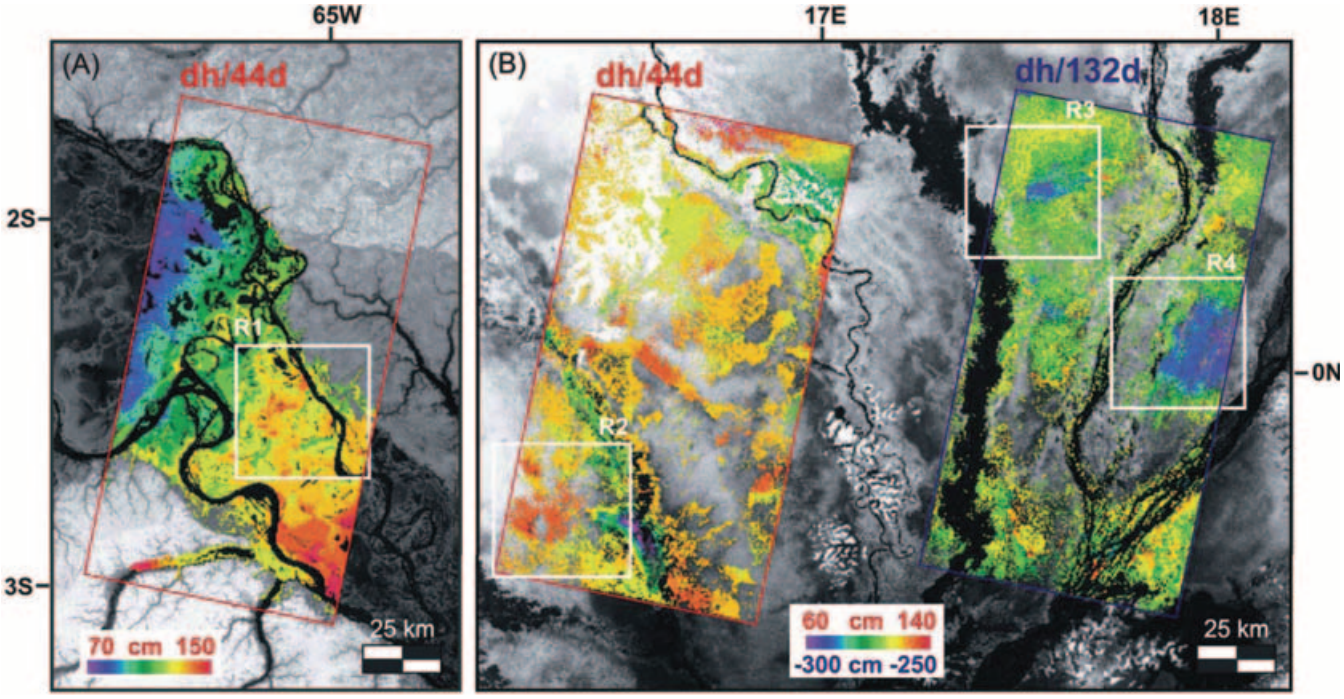

Figure 3. Measurements of changes in water level ($\partial h/\partial t$) superimposed on SRTM elevation maps in (A) Amazon and (B) Congo. Spatial patterns of temporal water level changes are measured from repeat-pass interferometric JERS-1 SAR. Acquisition dates of interferometric pairs are noted in Table 1. Locations without interferometric measurements were not flooded during at least one of the overpasses. This figure is available in colour online at www.interscience.wiley.com/journal/espl

Copyright © 2010 John Wiley & Sons, Ltd.

DOI: 10.1002/esp

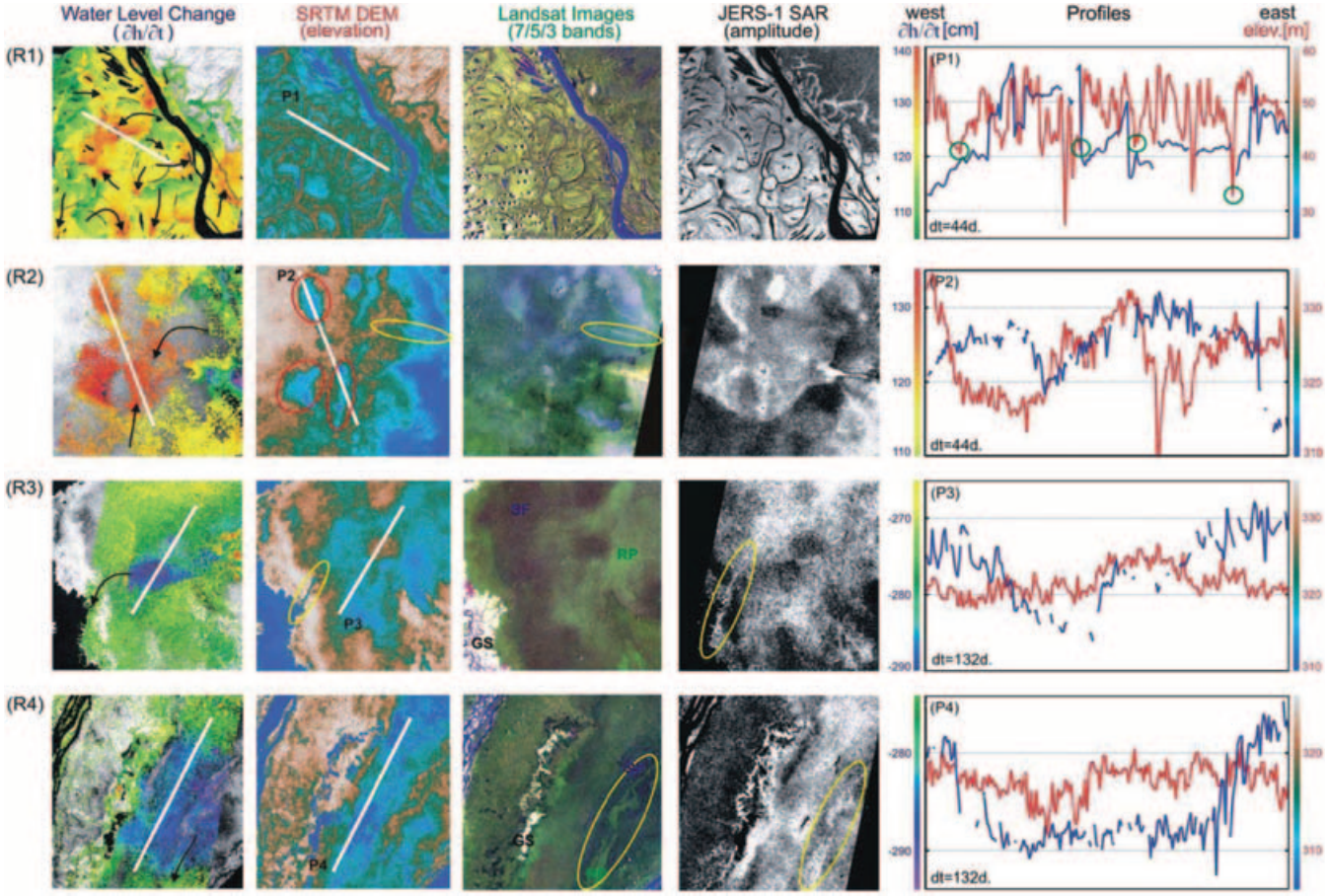

Figure 4. Detail of interferometric SAR measurements, SRTM elevations, Landsat color composite images (bands 7, 5, 3 shown in RGB), and JERS-1 amplitude images. Landsat acquisition dates are noted in Table 1. The close-up images all have the same spatial scale and have an elevation relief of 20–30 m. Black flow arrows are based on continuity with directions pointing toward areas of greater water accumulation at water increasing times in R1 and R2 and indicate evacuation directions at water decreasing times in R3 and R4. In the profiles, the red lines are topography and blue lines are interferometric $\partial h/\partial t$ measurements. Green circles note locations of floodplain channels, yellow ellipses note channels serving as pathways for water flow, and red ellipses note topographic depressions infilled by greater $\partial h/\partial t$ during rising water. In Congo regions R3 and R4, swamp forests, raphia palms, and grass savannas are marked with SF, RP, and GS, respectively. This figure is available in colour online at www.interscience.wiley.com/journal/espl

In summary, while the main flood wave moves downstream, floodplain channels deliver water with greater amounts to distinct, small pockets of the floodplain, in highly complex spatial patterns. Although these patterns seem to be associated with floodplain channels, predicting the spatial details of this pattern based on local SRTM topography is not straightforward.

Congo floodplain characterization

The two maps of $\partial h/\partial t$ for the Congo are shown in Figure 3. In contrast to the Amazon, there is no overall trend of increasing $\partial h/\partial t$ in the downstream direction. Indeed, it seems that at the scale of tens of kilometers, the spatial variability of Congo flooding is not directly relatable to distance downstream. In order to further characterize $\partial h/\partial t$ patterns, three smaller subsets within the two Congo study areas are isolated and are referred to hereafter as regions 2, 3, and 4, and are shown in Figure 4. While many flow directions are indicated in region 1 (in the Amazon), flow directions in regions 2, 3, and 4 are far more uniform. Thus, the uniformity of flow directions derived from the $\partial h/\partial t$ patterns indicate far less complex processes than for the Amazon, at spatial scales of hundreds of meters.

We hypothesize that these fundamental differences in the $\partial h/\partial t$ measurements between the Amazon and Congo floodplains are due to differences in the connectivity of the floodplain–river systems. From Figure 4, Landsat imagery and GRFM intensity in regions 2, 3, and 4 do not show the sinuous channels evident in region 1. Thus, our results suggest that connectivity of Congo River to the adjoining, interfluvial wetland areas is limited, compared with the Amazon. Furthermore, unlike the Amazon floodplain spatially limited by its *terre-firme*, the overall flooding pattern of the Congo does not have similarly distinct boundaries (see Figure 3).

Relationship between Congo hydraulics and topography

We carefully examined the relationship between our $\partial h/\partial t$ measurements and SRTM topography. The following examples in regions 2, 3, and 4 explore Congo flow hydraulics and relationships to topography. In region 2 both the Landsat and JERS-1 amplitude images show an overall, broad flooding pattern that covers the entire northern half of region 2 (e.g. regions of bright radar amplitudes). The $\partial h/\partial t$ measurements indicate a western area of flow convergence (arrows). However, SRTM topography over the same area contains both low and high elevations. In detail, $\partial h/\partial t$ values are greater within small, low-lying areas (red circles and profile P2, in region R2, Figure 4). The degree to which SRTM elevations are indicative of canopy or underlying topography is not clear in region 2. One channel is identified in the imagery and may represent a route for infilling of the interfluvial region.

Copyright © 2010 John Wiley & Sons, Ltd.

DOI: 10.1002/esp

In region 3, the $\partial h/\partial t$ measurements indicate a central area of flow divergence. No relationship is obvious between $\partial h/\partial t$ measurements and SRTM topography in profile P3 shown in Figure 4; we hypothesize that this may be due to differences in vegetation heights. Because radar returns are stronger in flooded vegetation, raphia palm areas (RP) in region 3 appear slightly more inundated than swamp forests, which are marked by slightly darker radar returns (SF; Laporte *et al.*, 1998). SRTM elevations can be associated with canopies and thus elevation variations in region 3 may be indicative of changes in vegetation heights. In region 3, grass savanna (GS) is essentially the ground height (305 m a.s.l.) and raphia palms are 10 m to 15 m in height, whereas swamp forest trees are taller, between 15 m and 20 m. In profile P3, the central portion is marked by swamp forests about 5 m higher than the raphia palms. Nearby grass savannas are about 15 m lower than the adjacent raphia palms. While the topography underlying the canopy is likely more subtle than indicated by SRTM, there does appear to be a small, ~5 m high ridge separating the Likouala-aux-Herbes River from the interfluvial areas to the north-east. This ridge is bisected by just one channel (yellow circle, Figure 4). Water level changes in region 3 are localized and decrease ~10 cm more in the middle than the edges of the 'bulls-eye' pattern in Figure 4. The $\partial h/\partial t$ values extend into the higher swamp forest, i.e. the 'island' along profile P3. Thus the degree to which SRTM topography is a control on water flow is not apparent (i.e. this 'island' of higher topography should not have an associated $\partial h/\partial t$ low). Within the interfluvial wetland area, the $\partial h/\partial t$ pattern is proximal to the isolated channel suggesting an evacuation route.

Similar to region 3, interfluvial topography in region 4 does not appear to be a control on $\partial h/\partial t$ patterns. Water level changes along profile P4 are not bounded by SRTM topography: $\partial h/\partial t$ values show the greatest change at the ends of the profile but SRTM topography shows essentially no bounding elevations. Like region 3, the $\partial h/\partial t$ spatial pattern is localized and adjacent to one channel (yellow circle) that connects with the mainstem Congo River.

In summary, our results suggest that flow patterns in the Congo are less governed by channel connectivity; flooded areas in the Congo study region are broadly distributed, lacking well-defined boundaries and do not appear to have abundant floodplain channels.

Braided River Characterization via SRTM Elevations for the Brahmaputra River

River basin storage and discharge are fundamental parameters in the terrestrial branch of the global water cycle. In particular, stream discharge represents a spatial and temporal integration of basin hydrology. At present the paucity of discharge measurements worldwide leaves uncertainties in our understanding of the hydrologic cycle. For example, this data insufficiency hinders flood prediction and water resources management in developing countries and ungaged basins (Hossain and Katiyar, 2006; Alsdorf and Lettenmaier, 2003). Limited water surface flow measurements from the terrestrial branch of the hydrologic cycle also restrict Global Climate Model parameterization and ocean circulation models (Roads *et al.*, 2003).

Measurements of surface water flow are most scarce in developing countries or inaccessible regions. Satellite remote sensing platforms have the ability to provide measurements necessary for estimating surface water flux that is required to understand the terrestrial branch of the hydrologic cycle. Spaceborne measurements have two primary advantages over *in situ* stream gage networks. First, they provide global coverage that is unrestricted by geopolitical boundaries, physically remote locations or by an institution's ability to maintain gages. Second, spaceborne measurements allow frequent and reliable measurements of surface water parameters (Alsdorf *et al.*, 2006). The SWOT mission proposes to measure water surface elevations globally (Alsdorf *et al.*, 2005). Our ability to use water surface elevations to estimate discharge must be assessed on a variety of fluvial geomorphologies in order to determine the applicability of such a satellite. In this section, we further demonstrate how these elevation measurements might be used to estimate stream discharge.

Prior efforts to estimate river discharge using spaceborne remote sensing data have utilized water surface elevations from the Shuttle Radar Topography Mission digital elevation model (SRTM DEM) to study the flow of single channel rivers such as the Amazon River (LeFavour and Alsdorf, 2005) and the Ohio River (Kiel *et al.*, 2006). In single channel rivers, relatively small changes in water surface height can yield large changes in discharge. Discharge estimation of braided rivers has primarily been studied in high latitude regions such as the Lena River, Siberia (Smith and Pavelsky, 2008) and the Peace–Athabasca Delta, Canada (Pavelsky and Smith, 2008). Brakenridge *et al.*, (2005, 2007) demonstrated that the Advanced Microwave Scanning Radiometer – Earth Observing System (AMSR-E) can estimate river discharge via measurements of inundated area. However, this research has focused on correlating *in situ* discharge measurements and river slope derived from topographic maps with remotely sensed width measurements (Smith *et al.*, 1996; Bjerklie *et al.*, 2005). Our approach is to measure the water surface elevation directly, rather than through indirect methods.

Study area

We selected the Brahmaputra River in South Asia to investigate the remote sensing of braided river discharge estimation for the following reasons. (1) It is a sand bed, braided river. Prior studies using remote sensing to estimate discharge have looked at either braided rivers in glacial outflows or single channel rivers. (2) Its morphology is typical of lowland braided rivers such as the Congo River in West Africa and the Yellow River in China. Thus, the results gained from this study should have broader applicability. *In situ* data includes bathymetric cross-sections and *Q* measurements, which are available from the Bangladesh Institute of Water Modeling (BIWM) MIKE-11 database (BIWM, 2007, unpublished data). Our study area is shown in Figure 5.

The Brahmaputra River is an International River Basin with complex water sharing issues. Bangladesh contains three major trans-boundary rivers (Ganges, Brahmaputra and Meghna) that account for a majority of the surface water flow during the Monsoon season. Yet only 8% of the combined basin area is contained within the country borders (Paudyal, 2002). Flood prediction in Bangladesh is hindered by the lack of discharge measurements available for upstream reaches outside of Bangladesh. Bangladesh is only able to provide 2–3 days of warning by monitoring river stage located inside the 8% of the total basin area (Hossain and Katiyar, 2006). The remote sensing of surface water elevations may provide basin-wide key observations in flood prediction and hydrologic modeling, thus providing some advanced warning regarding potential flood hazards, as well as knowledge of typical flow regimes.

Copyright © 2010 John Wiley & Sons, Ltd.

DOI: 10.1002/esp

Flow hydraulics

Manning's Equation yields water flow velocity as the product of water surface slope ($\partial h/\partial x$), hydraulic radius (R) and the roughness coefficient (n); see Albertson and Simmons (1964). It is an empirical equation, but nevertheless well used in the hydrological sciences and in remote sensing estimates of discharge (Bjerklie *et al.*, 2005; LeFavour and Alsdorf, 2005). Multiplying flow velocity by channel cross-sectional (A) area yields discharge:

$$Q = \frac{1}{n} R^{2/3} \left(\frac{\partial h}{\partial x} \right)^{1/2} A \quad (1)$$

The Brahmaputra River is sand bedded, without vegetation. Values of the roughness coefficient for such geomorphologies are estimated to range from 0·018 to 0·035 (Ashworth *et al.*, 2000; Albertson and Simons, 1964). Following Albertson and Simons (1964), we selected a value of n equal to 0·025 for natural streams in fair condition. The roughness coefficient may be used as an adjustment factor to reduce discharge error in future applications.

The fundamental difference in flow hydraulics between discharge estimation using river slope on single channel rivers versus multi-channel braided rivers is bank cohesiveness. Increasing discharge in a single channel river results in increasing water surface elevation. Increasing discharge in a braided river largely results in increases in river width (Mosley, 1982). When using water surface slope and Manning's Equation to estimate discharge in braided rivers, the wide and shallow river geometry may increase errors associated with estimating A and R.

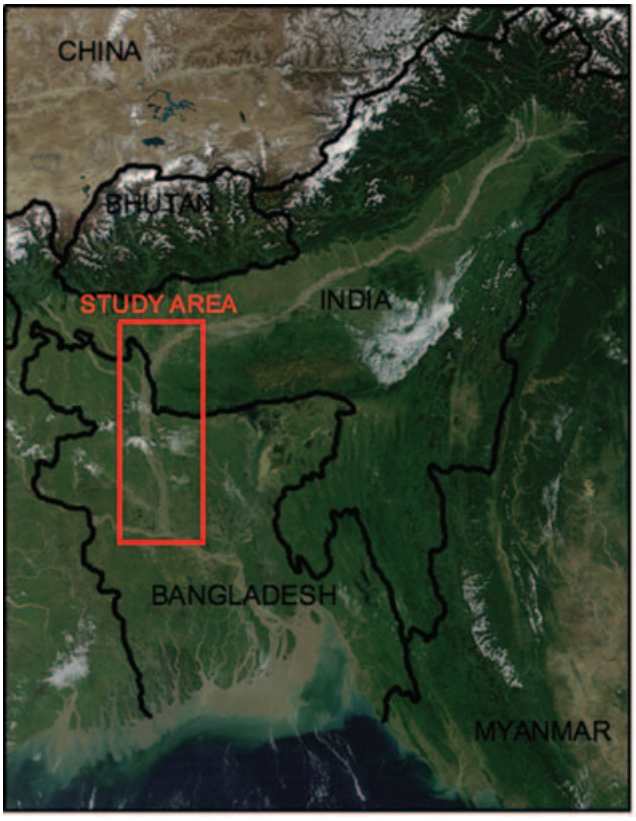

Figure 5. Brahmaputra River region in South Asia. This figure is available in colour online at www.interscience.wiley.com/journal/espl

Remote sensing and in situ data sources

The SRTM DEM yields water surface elevations where wind roughening and waves allow radar backscattering. This results from SRTM's large radar look angle and C-band frequency (Smith and Alsdorf, 1998). Essentially, water surfaces are specular reflectors, which cause radar echoes emitted at the large off-nadir angles of SRTM to reflect away from the antennae. Roughened water surfaces, however, provide sufficient scattering of the radar echoes that some energy returns to the antennae providing a height measurement of the water surface.

The SRTM DEM does not explicitly distinguish between land pixels and water pixels. This separation was accomplished by preparing a land/water classification mask from two Landsat 7 images acquired on 19 February 2000. This date falls within the SRTM DEM data acquisition period of 7–21 February 2000. The Brahmaputra River channel position may change up to 1 km per year (Coleman, 1969); therefore it is imperative that land/water classification data sources come from as close to SRTM DEM acquisition dates as possible. Classification was accomplished using an ISODATA algorithm. Many bars and shallows areas were not resolved by the 30 m resolution Landsat image. However, because water surface slope was averaged across approximately 100 km of flow distance the percentage error caused by misclassification was minimized.

The land/water classification mask was used to create a spatial grid for associating all hydraulic parameters with their position along the river. The land/water classification mask covered a total of 258 km of flow distance. The land/water mask and SRTM elevations are shown in Figure 6.

Hydraulic radius (R) and cross-sectional area of flow (A) were estimated using bathymetric cross-sectional measurements from the BIWM MIKE-11 database. Prior to the onset of the following year's monsoon, BIWM updates the river bathymetry for the major rivers every 5 km of the river reach through an intensive field campaign. For a constantly moving channel system like the Brahmaputra, this probably represents the most accurate *in situ* data available for a braided river. These river cross-sections map the channel morphology at fixed locations but do not indicate river stage during the SRTM data acquisition period. The water surface elevation at the flow distance of each cross-section is determined by fitting a first-degree polynomial to the SRTM DEM water elevations. R and A are then calculated with this knowledge of bathymetric elevation and water surface elevation; this is illustrated in the schematic in Figure 7. Cross-sectional measurements were obtained in 1997 and 1998. This discrepancy from the SRTM

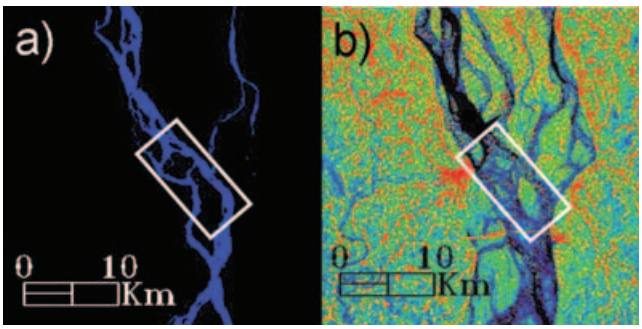

Figure 6. Example of radar return due to water surface roughening. Frame A shows the land/water classification mask with a box displaying a section of river convergence to two channels. This same section is contained in the box in Frame B, which shows the SRTM DEM. Water surface roughening allows radar return and measurement of water surface elevation. This figure is available in colour online at www.interscience.wiley.com/journal/espl

Copyright © 2010 John Wiley & Sons, Ltd.

DOI: 10.1002/esp

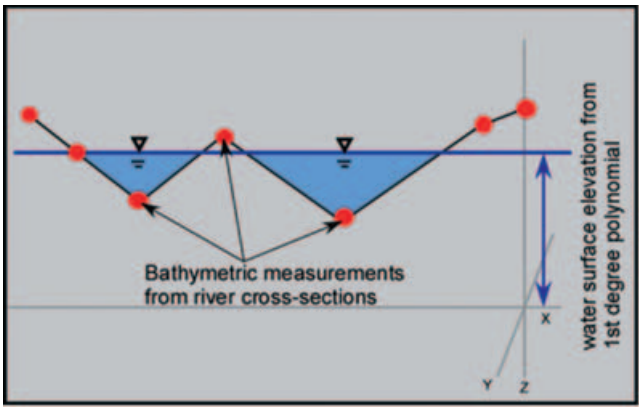

Figure 7. Schematic of channel cross-sectional geometry. The blue line indicates the water surface elevation at a given bathymetric cross-section during February 2000. The orange points represent *in situ* elevation measurements of the channel bathymetry. These two elevations are used along with the distance between bathymetric measurements to calculate cross-sectional area and hydraulic radius. This figure is available in colour online at www.interscience.wiley.com/journal/espl

data acquisition period is a source of error in discharge measurements.

Hydraulic parameters and discharge estimation

Water surface slope

Bangladesh experiences a monsoon climate, resulting in a yearly dry and very wet season. The SRTM DEM data acquisition period falls during the dry season; therefore, slope anomalies caused by propagating flood waves are not expected. The resultant water surface elevations from ~250 km of flow distance and the associated first-degree polynomial fit line are displayed in Figure 8. Water surface slope was derived by fitting a first-degree polynomial to SRTM DEM water surface elevations collected from the entire river length in our land/water classification mask. The standard deviation, σ, of water surface elevations after removing the first-degree trend is 5·8 m. Because water surfaces do not vary sharply from pixel-to-pixel, the standard deviation is taken to represent measurement error. We estimate the minimum reach length required to determine river slope via the equation from LeFavour and Alsdorf (2005): $\text{Reach Length}_{\text{minium}} = 2\sigma / \text{Slope}_{\text{minium}}$. We assumed the slope of our first-degree polynomial fit to be the Brahmaputra River's minimum slope because our measurements are from the yearly low flow stage. Without measurements of river slope changes, this is considered a general estimate. This implies that a minimum reach length is of 138 km is required to distinguish changes in slope along the flow distance (i.e. only linear fits are valid for reach lengths less than 138 km whereas two linear fits or second-order polynomials are valid for lengths greater than 138 km).

Discharge estimation

We use stream gage discharge estimates to determine the accuracy of our SRTM based estimate of Q. There is only one available gage measurement contained in the study area that had flow measurements matching very closely with the SRTM DEM overflight period. There are no major tributaries or distributaries within the flow distance region of 12 km upstream and 12 km downstream of this gage. Thus, we assume that the river discharge will be approximately constant in this section of the river. Four cross-sections (Figure 7) fall within this 24 km flow distance. These cross-sectional geometries were combined with the SRTM based water surface slope (Figure 8) to estimate Q. The discharge estimates at these cross-sections are within 1200 $m^3 s^{-1}$ of the *in situ* gage measurement (Figure 9). Averaging the four Q estimates and using the *in situ* measurement as 'truth', the average difference represents an error of 2·3%.

The total flow distance covered by the land/water classification mask is 258 km. For the slope input to Manning's Equation, two separate first-degree polynomial fits were calculated for the upper and lower reach of the river (Figure 10). This allows a more accurate, localized slope estimate. The downstream half was best fit with a first degree line using a slope of 10 cm km^{-1}, while the upstream half was fit with a first degree line with a slope of 9·7 cm km^{-1}.

Figure 11 shows the resulting Q estimations at each of the 35 river cross-sections. Q increases along the flow distance as expected due to tributary input. However, because our estimation occurs during the dry (pre-Monsoon) season this increase is slight.

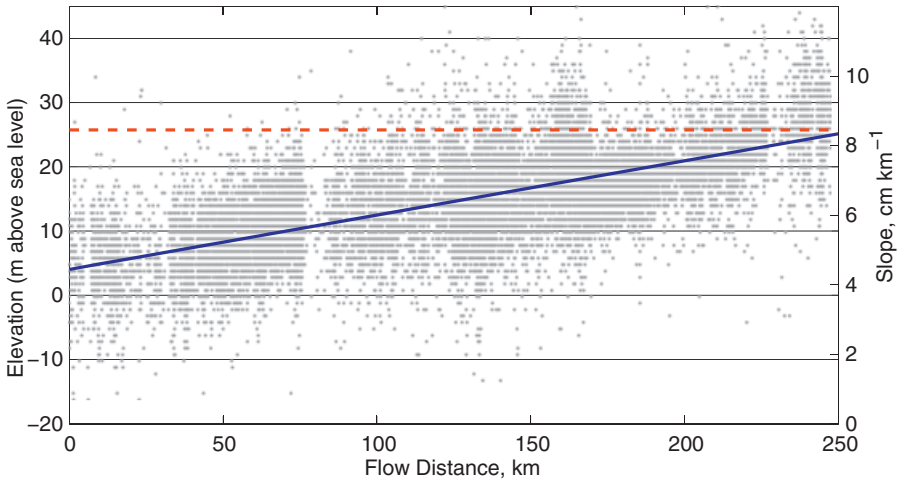

Figure 8. Water surface elevations (closed circles) with a first degree polynomial (solid line) fit to the entire ~250 km of river reach. The slope of the polynomial (dashed line) is also shown. This figure is available in colour online at www.interscience.wiley.com/journal/espl

Copyright © 2010 John Wiley & Sons, Ltd.

DOI: 10.1002/esp

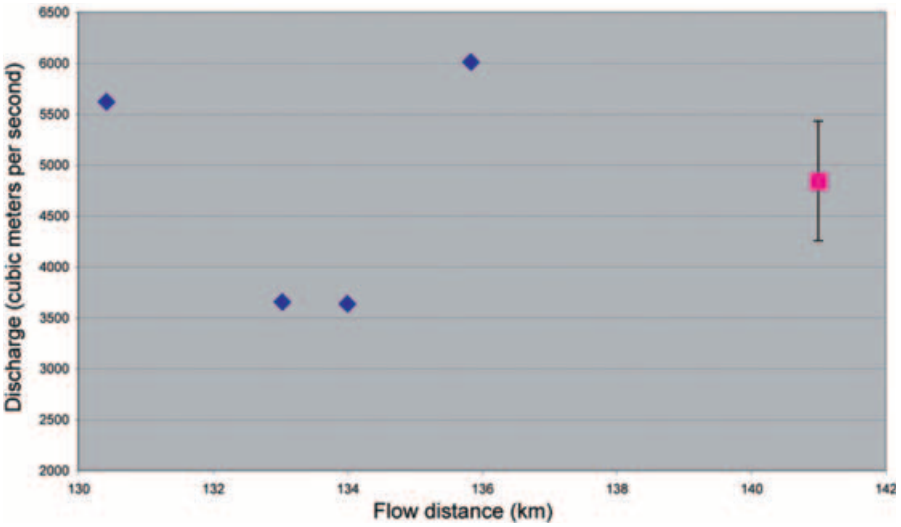

Figure 9. Diamonds indicate discharge estimation using the Manning's Equation for cross-sections nearest the river gage. The square indicates the river gage discharge measurement, with error bars showing the standard deviation of discharge measurements for January 2000. This figure is available in colour online at www.interscience.wiley.com/journal/espl

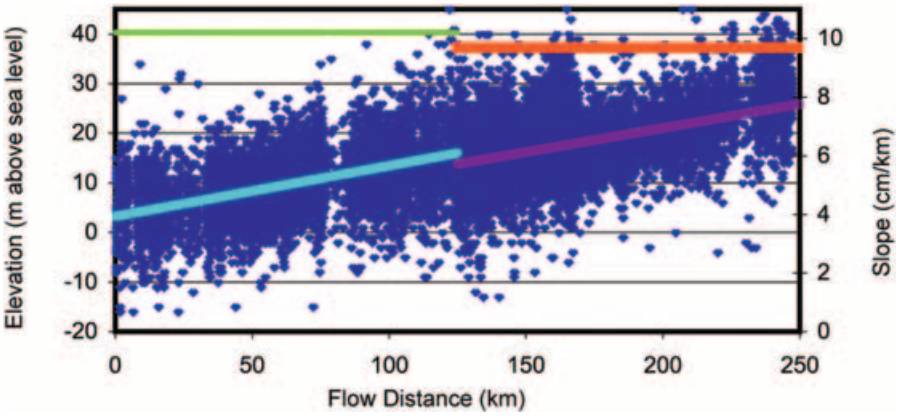

Figure 10. Water surface elevations with two first degree fit lines. A slight increase in river slope occurs with downstream flow distance. This figure is available in colour online at www.interscience.wiley.com/journal/espl

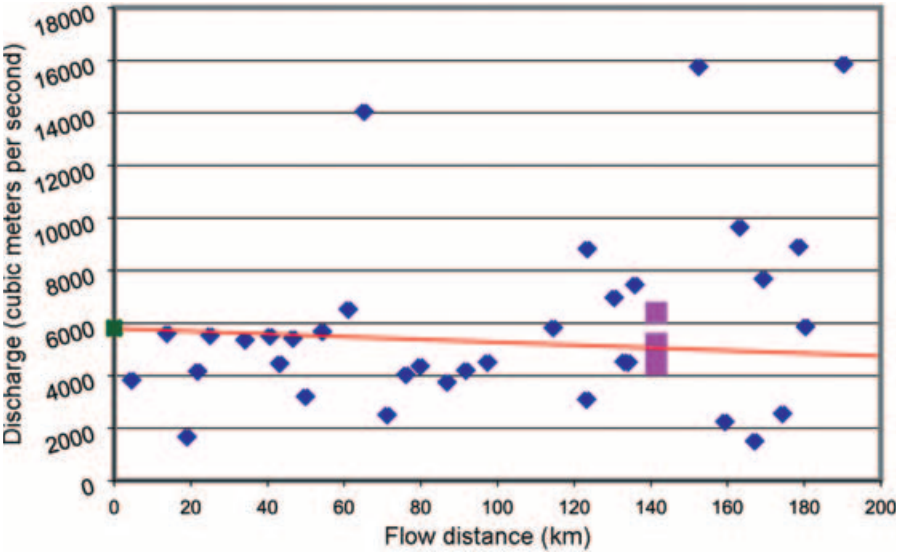

Figure 11. Discharge estimations at each river cross section (diamonds). The line indicates the trend between February 2000 gage measurements and the low-flow average at the Brahmaputra's mouth (squares) as reported in Ashworth *et al.* (2000). This figure is available in colour online at www.interscience.wiley.com/journal/espl

Copyright © 2010 John Wiley & Sons, Ltd.

DOI: 10.1002/esp

Conclusions

We have performed two experiments, which together illustrate the potential of SWOT measurements of temporal variations ($\partial h/\partial t$) and spatial variations ($\partial h/\partial x$) of water levels to characterize complex fluvial processes. First, interferometric SAR techniques were used to estimate $\partial h/\partial t$ over the Congo and Amazon River floodplains. These $\partial h/\partial t$ measurements indicate very different fluvial processes at work. The many Amazon floodplain channels with identifiable connections to the mainstem contrast sharply with the more sparse connections between Congo rivers and interfluvial areas. Essentially, the scale and magnitude of floodplain building processes in the Amazon are not similarly found in the Congo. Moreover, our results suggest that a straightforward relationship is not apparent between SRTM topography and Amazon or Congo flow hydraulics.

Second, SRTM topography measurements over the braided Brahmaputra River were used to derive channel slope, $\partial h/\partial x$. In combination with *in situ* bathymetry measurements, water elevation and slope allow for discharge estimation. The low spatial resolution and large height error associated with the SRTM DEM hinders the accuracy of this estimation. The use of bathymetric cross-sections was required to accurately estimate cross-sectional area and hydraulic radius. However, much like discharge measurements, such cross-sections are not available in all rivers. One potential solution to this problem is to determine the relationship between river width and hydraulic radius. This would allow all hydraulic parameters necessary for estimating discharge from remotely sensed hydraulic parameters. These results suggest that a wide-swath satellite altimeter designed to measure water surface elevations could produce basin wide discharge estimations within a reasonable confidence level where *in situ* gage data are not available. Such discharge estimations, as anticipated from SWOT, would not be limited by geopolitical boundaries or human access and therefore stand to vastly improve flood forecasting in international river basins. SWOT data will be an improvement on the proxy data from JERS and SRTM used in this study. Instead of the one-time SRTM measurement of river slope, SWOT would measure river slope ($\partial h/\partial x$) approximately weekly at mid-latitudes, with a minimum of two measurements per 22-day orbital cycle for equatorial regions (Biancamaria *et al.*, 2009). SWOT precision would be centimetric, of the same order as the precision of the JERS $\partial h/\partial t$ measurements; thus SWOT would essentially combine the strengths of JERS and SRTM datasets used in this study.

Acknowledgements—This study was funded by the Ohio State University's Climate, Water, and Carbon program, NASA's Terrestrial Hydrology program, NASA's Physical Oceanography Program, and the Korea Science and Engineering Foundation. We thank Nadine Laporte for sharing her knowledge of Congo vegetation. JAXA supplied the JERS-1 data. Landsat data is from the Global Land Cover Facility. *In situ* data for the Brahmaputra river was available as part of a 5-year Memorandum of Understanding between Tennessee Technological University and BIWM for research collaboration and staff training. Land-water classification of Landsat data was supported by the NASA Rapid Prototyping Capability (RPC) program.

References

Aalto RL, Dunne T, Montgomery DR, Nittrouer CA, Guyot J. 2003. Episodic sediment accumulation on Amazonian flood plains influenced by El Nino/Southern Oscillation. *Nature* **425**: 493–497.

Albertson ML, Simons BB. 1964. Section 7: Fluid mechanics. In *Handbook of Applied Hydrology: A Compendium of Water-Resources Technology*, Chow VT (ed). McGraw-Hill: New York.

Alsdorf DE, Melack JM, Dunne T, Mertes LAK, Hess LL, Smith LC. 2000. Interferometric radar measurements of water level changes on the Amazon floodplain. *Nature* **404**: 174–177.

Alsdorf, DE. 2003. Water storage of the central amazon floodplain measured with GIS and remote sensing imagery. *Annals of the Association of American Geographers* **93**: 55–66.

Alsdorf DE, Lettenmaier DP. 2003. Tracking fresh water from space *Science* **301**: 1491–1494.

Alsdorf DE, Rodriguez E, Lettenmaier D, Famiglietti J. 2005. WatER: The Water Elevation Recovery Satellite Mission, a Response to the National Research Council Decadal Survey Request for Information, URL: http://www. bprc.osu.edu/water/.

Alsdorf DE, Rodriguez E, Lettenmaier DP. 2006. Measuring surface water from space. **45**: RG2002, doi:10.1029/2006RG000197.

Alsdorf D, Bates P, Melack J, Wilson M, Dunne T. 2007. Spatial and temporal complexity of the Amazon flood measured from space. *Geophysical Research Letters* **34**: L08402.

Ashworth PJ, *et al*. 2000. Morphological evolution and dynamics of a large, sand braid-bar, Jamuna River, Bangladesh. *Sedimentology* **47**: 533–555.

Bangladesh Institute of Water Modeling. 2007. Discharge data. http://www.iwmbd.org/.

Biancamaria S, Andreadis KM, Durand M, Clark EA, Rodriguez E, Mognard NM, Alsdorf DE, Lettenmaier DP, Oudin Y. 2009. Preliminary characterization of SWOT hydrology error budget and global capabilities, *IEEE Journal of Selected Topics in Applied Earth Observations and Remote Sensing*, DOI: 10.1109/JSTARS.2009.2034614.

Birkett CM, Mertes AAK, Dunne T, Costa MH, Jasinski MJ. 2002. Surface water dynamics in the Amazon Basin: application of satellite radar altimetry. *Journal of Geophysical Research* **107**: doi:10.1029/2001JD000609.

Bjerklie DM, Moller D, Smith LC, Dingman SL. 2005. Estimating discharge in rivers using remotely sensed hydraulic information. *Journal of Hydrology* **309**: 191–209. DOI: 10.1016/l.lhydrol.2004.11.022

Brakenridge GR, Nghiem SV, Anderson E, Chien S. 2005. Space-based measurement of river runoff. *EOS Transactions AGU* **86**(19): 185, 188.

Brakenridge GR. Nghiem SV, Anderson E, Mic R. 2007.Orbital microwave measurement of river discharge and ice status. Water Resources Research **43** (W04405). DOI.: 10.1029/2006WR005238.

Calmant S, Seyler F. 2006. Continental surface waters from satellite altimetry. *Comptes Rendus Geoscience* **338**: 111–1122.

Campbell D. 2005. *The Congo River basin, The World's Largest Wetlands: Ecology and Conservation*. Cambridge University Press; 149–165.

Coleman JM. 1969. The Brahmaputra River: channel processes and sedimentation. *Sediment Geology* **3**: 129–139.

De Grandi GD, Mayaux P, Rauste Y, Rosenqvist A, Simard M, Saatchi SS. 2000. The global rain forest mapping project JERS-1 radar mosaic of tropical Africa: development and product characterization aspects. *IEEE Transactions of Geoscience and Remote Sensing* **38**: 2218–2233.

Farr T *et al*. 2007. The Shuttle Radar Topography Mission. *Reviews of Geophysics* **45**: RG2004, doi:10.1029/2005RG000183.

Frappart F, Papa F, Famiglietti JS, Prigent C, Rossow WB, Seyler F. 2008, Interannual variations of river water storage from a multiple satellite approach: a case study for the Rio Negro River basin. *Journal of Geophysical Research* **113**: doi:10.1029/2007JD009438.

Frappart F, Seyler F, Martinez JM, León JG, Cazenave A. 2005. Floodplain water storage in the Negro River basin estimated from microwave remote sensing of inundation area and water levels. *Remote Sensing of the Environment* **99**: 387–399.

Hess LL, Melack JM, Novo EM, Barbosa CCF, Gastil M. 2003. Dual-season mapping of wetland inundation and vegetation for the central Amazon basin. *Remote Sensing of the Environment* **87**: 404–428.

Hossain, F Katiyar N. 2006. Improving flood forecasting in international river basins. *EOS Transactions AGU* **87**(5): 49,54.

Jung HC, Alsdorf D. In press. Repeat-pass multi-temporal interferometric SAR coherence variations with Amazon floodplain and lake

Copyright © 2010 John Wiley & Sons, Ltd.

habitats. *International Journal of Remote Sensing*. DOI: 10.1080/01431160902902609

Kazadi S-N, Kaoru F. 1996. Interannual and long-term climate variability over the Zaire River Basin during the last 30 years. *Journal of Geophysical Research* **101**: 21351–21360.

Kiel B, Alsdorf DE, LeFavour G. 2006. Capability of SRTM C- and X-band DEM data to measure water elevations in Ohio and the Amazon. *Photogrammic Engineering and Remote Sensing* **72**: 313–320.

Koblinsky CJ, Clarke RT, Brenner AC, Frey H. 1993. Measurement of river level variations with satellite altimetry. Water Resources Research **29**(6): 1839–1848.

Kouraev AV, Zakharova EA, Samain O, Mognard NM, Cazenave C. 2004. Ob river discharge from TOPEX/Poseidon satellite altimetry (1992–2002). *Remote Sensing of the Environment* **93**: 238–245.

Laporte N, Goetz SJ, Justice CO, Heinicke M. 1998. A new land cover map of central Africa derived from multi-resolution, multi-temporal AVHRR Data. *International Journal of Remote Sensing* **19**: 3537–3550.

Laraque A, Mahe G, Orange D, Marieu B. 2001. Spatiotemporal variations in hydrological regimes within Central Africa during the XXth century. *Journal of Hydrology* **204**: 104–117.

Lee H, Shum CK, Yi Y, Braun A, Kuo CK. 2008. Laurentia crustal motion observed using TOPEX/POSEIDON radar altimetry over land. *Journal of Geodynamics* **46**: 182–193.

Leon JG, Calmant S, Seyler F, Bonnet M-P, Cauhope M, Frappart F, Filzola N, Fraizy P. 2006. Rating curvers and estimation of average water depth at the upper Negro River based on satellite altimeter data and modeled discharges. *Journal of Hydrology* **328**: 481–496.

LeFavour G, Alsdorf DE. 2005. Water slope and discharge in the Amazon River estimated using the shuttle radar topography mission digital elevation model. *Geophysical Research Letters* **32**: L17404, DOI:10.1029/2005GL023836.

Massonnet D, Rossi M, Carmona C, Adragna F, Peltzer G, Feigl K, Rabaute T. 1993. The displacement field of the Landers earthquake mapped by radar interferometry. *Nature* **364**: 138–142.

Melack JM, Forsberg BR. (2001). Biogeochemistry of Amazon floodplain lakes and associated wetlands. In *The Biogeochemistry of the Amazon Basin and its Role in a Changing World*, Oxford University Press: New York; 235–276.

Mertes LAK, Dunne T, Martinelli LA. 1996. Channel-floodplain geomorphology along the Solimoes-Amazon River, Brazil. *GSA Bulletin* **108**: 1089–1107.

Mosley MP. 1982. Analysis of the effect of changing discharge on channel morphology and instream uses in a braided river, Ohau River, New Zealand. Water Resources Research **18**(4): 800.

National Research Council (NRC). 2007. *Earth Science and Applications from Space: National Imperatives for the Next Decade and Beyond*. The National Academies Press: Washington DC. P.418.

Paudyal GN. 2002. Forecasting and warning of water-related disasters in a complex hydraulic setting: the case of Bangladesh (Prévision et annonce de catastrophes hydrologiques en contexte hydraulique complexe. Le cas du Bangladesh). *Hydrological Sciences Journal* **47**: S5–S18.

Pavelsky TM, Smith LC. 2008. Remote sensing of hydrologic recharge in the Peace-Athabasca Delta, Canada, *Geophysical Research Letters* **35**, L08403, doi:10.1029/2008GL033268.

Roads J, *et al*. 2003. GCIP water and energy budget synthesis (WEBS). *Journal of Geophysical Research* **108**: D16, 8609, DOI:10.1029/2002JD002583.

Rosenqvist A, Birkett CM. 2002. Evaluation of JERS-1 SAR mosaics for hydrological applications in the Congo River basin. *Internation Journal of Remote Sensing* **23**: 1283–1302.

Sautter G. 1966. De l'Atlantique au fleuve Congo: Une géographie du sous-peuplement (Paris/La Haye: Mouton), 2.

Sippel SJ, Hamilton SK, Melack JM. 1992. Inundation area and morphometry of lakes on the Amazon River floodplain, Brazil. *Archives of Hydrobiology* **123**: 385–400.

Siqueira P, Chapman B, McGarragh G. 2003. The coregistration, calibration, and interpretation of multiseason JERS-1 SAR data over South America. *Remote Sensing of the Environment* **87**: 389–403.

Smith LC, Pavelsky TM. 2008. Estimation of river discharge, propagation speed, and hydraulic geometry from space: Lena River, Siberia. *Water Resources Research* **44**: W03427, doi:10.1029/2007WR006133.

Smith LC, Alsdorf DE. 1998. Control on sediment and organic carbon delivery to the Arctic Ocean revealed with space-borne synthetic aperture radar: Ob' River, Siberia. *Geology* **26**: 396–298.

Smith LC, Isacks BL, Bloom AL, Murray AB. 1996. Estimation of discharge from three braided rivers using synthetic aperture radar satellite imagery: Potential application to ungaged basins. *Water Resources Research* **32**(7): 2021–2034.

Copyright © 2010 John Wiley & Sons, Ltd.